INSTITUTE OF PHYSICS PUBLISHING PLASMA PHYSICS AND CONTROLLED FUSION

Plasma Phys. Control. Fusion **43** (2001) A141–A150 PII: S0741-3335(01)28146-9

Nonlinear electromagnetic gyrokinetic simulations of tokamak plasmas

F Jenko[1] **and W Dorland**[2]

[1] Max-Planck-Institut für Plasmaphysik, EURATOM Association, 85748 Garching, Germany
[2] University of Maryland, College Park, MD 20742, USA

Received 22 June 2001
Published 22 November 2001
Online at stacks.iop.org/PPCF/43/A141

Abstract

One of the central physics issues currently targeted by nonlinear gyrokinetic simulations is the role of finite-β effects. The latter change the MHD equilibrium, introduce new dynamical space and time scales, alter and enlarge the zoo of electrostatic microinstabilities and saturation mechanisms, and lead to turbulent transport along fluctuating magnetic field lines. It is shown that the electromagnetic effects on primarily electrostatic microinstabilities are generally weakly or moderately stabilizing. However, the saturation of these modes and hence the determination of the transport level in the quasi-stationary turbulent state can be dominated by nonlinear electromagnetic effects and yield surprising results. Despite this, the induced transport is generally electrostatic in nature well below the ideal ballooning limit.

1. Introduction

Besides its immense importance in many fields of science and engineering, turbulence is a fundamental example of nonlinear dynamics in open systems. It generally develops a quasi-stationary state far from thermodynamic equilibrium. The best known example is three-dimensional fluid turbulence. Here, the decay process of larger vortices into smaller ones can be described in terms of an energy cascade in wavenumber space. Energy injected into such a system at large length scales is redistributed by nonlinear interactions, cascading through a wide range of inertial scales and is eventually dissipated at very small scales by viscosity [1].

Turbulence in magnetized plasmas differs in several significant ways [2]. The strong external magnetic field leads to a pronounced anisotropy of the turbulent fluctuations. Whereas the dynamics parallel to the magnetic field lines is that of an unmagnetized plasma, the perpendicular dynamics is described by drifts. This leads to vortices whose parallel to perpendicular correlation length ratio is of the order of 10^2–10^4. In the perpendicular planes, the dynamics sometimes resembles two-dimensional fluid turbulence whose energy cascade is directed to *larger* spatial scales, describing merging vortices. This may contribute to the drive of larger-scale structures such as 'zonal flows' (purely poloidal flows).

Plasma turbulence is complicated by effects from Landau resonances, trapped particles, and finite gyroradii which make a kinetic treatment inevitable. This is true even in the edge region of many tokamaks (inside the last-closed flux surface) [3, 4] which is often described by Braginskii-type fluid models. In particular the absence of Landau resonance effects which destabilize electron drift waves in the weakly collisional limit and the overestimate of the parallel thermal conductivities can yield spurious results in certain parameter regimes. Therefore, despite the usefulness of Braginskii-type models, gyro-Landau-fluid (GLF) models [5] or gyrokinetic models [6] are needed to be able to accurately describe all regimes of both core and edge turbulence on closed field lines.

In the following, it will be attempted to give an overview of the present status of nonlinear electromagnetic gyrokinetic simulations of tokamak plasmas. The new physics introduced by finite-β effects includes the coupling of primarily electrostatic instabilities to kinetic shear Alfvén waves, the occurrence of inherently electromagetic instabilities, and turbulent transport along fluctuating magnetic field lines. In addition, 'zonal magnetic fields' (turbulence-generated fluctuating components of the poloidal magnetic field) can modulate the q profile and thus shear-stabilize the turbulence.

2. Gyrokinetic simulations of plasma turbulence

2.1. Gyrokinetic equation

Kinetic equations (in the collisionless limit) can generally be written as

$$(\partial_t + \dot{\boldsymbol{z}} \cdot \nabla_z) f(\boldsymbol{z}, t) = 0 \tag{1}$$

where $f(\boldsymbol{z}, t)$ is a distribution function depending on the phase-space coordinates $\boldsymbol{z}$ and time t. One obtains the well known Vlasov equation by specifying

$$\dot{\boldsymbol{x}} = \boldsymbol{v} \qquad \dot{\boldsymbol{v}} = \frac{e}{m}\left(\boldsymbol{E} + \frac{\boldsymbol{v}}{c} \times \boldsymbol{B}\right) \tag{2}$$

where f depends on the particle coordinates $\boldsymbol{z} = (\boldsymbol{x}, \boldsymbol{v})$. This equation is nonlinear since the electromagnetic fields depend on f through Maxwell's equations. In principle, it could be used to describe turbulent fluctuations in collisionless plasmas, but that would require a numerical space–time resolution way beyond the scales of interest which are characterized by [6]

$$\frac{\tilde{f}}{f_0} \sim \frac{e\tilde{\phi}}{T} \sim \frac{\tilde{A}_\parallel}{B\rho} \sim \frac{\omega}{\Omega} \sim \frac{\rho}{L} \ll 1 \qquad k_\parallel L \sim k_\perp \rho \sim 1 \tag{3}$$

where $\tilde{f}$ is the perturbed distribution function, f_0 is the equilibrium distribution function, $\tilde{\phi}$ and $\tilde{A}_\parallel$ are the perturbed parts of the electrostatic and parallel vector potential, B is the equilibrium magnetic field, L is an equilibrium scale length (of density, temperature, or magnetic field), $\Omega = (eB)/(mc)$ and $\rho = v_\mathrm{t}/\Omega$ are the cyclotron frequency and thermal gyroradius of a given particle species with thermal velocity $v_\mathrm{t}^2 = T/m$ and charge e. Based on this ordering, a gyroaveraged Vlasov equation for the gyrocentre coordinates $\boldsymbol{z} = (\boldsymbol{R}, v_\parallel, \mu)$ was derived in the 1980s by various authors [6–9]. The corresponding equations of motion are

$$\dot{\boldsymbol{R}} = v_\parallel \tilde{\boldsymbol{b}} + \boldsymbol{v}_E + \boldsymbol{v}_\mathrm{d} \qquad \dot{v}_\parallel = \frac{e}{m} E_\parallel - \frac{\mu}{m} \tilde{\boldsymbol{b}} \cdot \nabla B + v_\parallel (\boldsymbol{b} \cdot \nabla \boldsymbol{b}) \cdot (\boldsymbol{v}_E + \boldsymbol{v}_\mathrm{d}) \tag{4}$$

where the magnetic moment $\mu = (m v_\perp^2)/(2B)$ is a constant of motion, while

$$\tilde{\boldsymbol{b}} = \boldsymbol{b} + \frac{1}{B} \nabla \times (\bar{A}_\parallel \boldsymbol{b}) \tag{5}$$

denotes the unit vector along the total (fluctuating) magnetic field,

$$\boldsymbol{v}_E = \frac{c}{B}\boldsymbol{b} \times \nabla\bar{\phi} \qquad \boldsymbol{v}_{\mathrm{d}} = \frac{v_\parallel^2}{\Omega}\boldsymbol{b} \times (\boldsymbol{b} \cdot \nabla\boldsymbol{b}) + \frac{\mu}{m\Omega}\boldsymbol{b} \times \nabla B \tag{6}$$

are the $E \times B$ drift velocity and the combined curvature and ∇B drift velocity, and

$$E_\parallel = -\tilde{\boldsymbol{b}} \cdot \nabla\bar{\phi} - \frac{1}{c}\partial_t \bar{A}_\parallel \tag{7}$$

is the parallel electric field. The overbar denotes the averaging of the fluctuating potentials over a gyro orbit whose radius is set by μ. This procedure is necessary because $\boldsymbol{R}$ describes the location of the gyrocentre, not that of the particle itself. Therefore a gyrocentre at $\boldsymbol{R}$ does not feel $\phi(\boldsymbol{R})$ but $\bar{\phi}(\boldsymbol{R})$. (Note that the above equations are sometimes written in terms of $\boldsymbol{b}^* = \boldsymbol{b} + (v_\parallel/\Omega)\boldsymbol{b} \times (\boldsymbol{b} \cdot \nabla\boldsymbol{b})$ instead of $\boldsymbol{b}$. This formulation is equivalent to the one above since the curvature drift velocity and the last term is the $\dot{v}_\parallel$ equation are hidden in $\boldsymbol{b}^*$.) Equations (4)–(7) are complemented by the gyroaveraged Maxwell's equations [6–9]. The advantages of this gyroaveraged formulation for numerical investigations are at hand. One independent variable (corresponding to the gyrophase) has been removed, and one of the remaining variables, μ, enters the equations only as a parameter which reduces the associated numerical effort. Moreover, the space–time resolution requirements are relaxed considerably. On the other hand, all relevant kinetic effects are retained in a non-perturbative way. Attempts to further reduce the numerical demands by integrating out the velocity space dynamics (leading to a GLF description) have proven to be challenging though helpful. It is generally agreed upon that the gyrokinetic Vlasov–Maxwell system constitutes the best starting point for accurate yet efficient simulations of collisionless turbulence in tokamaks.

2.2. Computational issues

Kinetic equations can be solved numerically by a number of algorithms which can be roughly divided into two groups corresponding to the Lagrangian and Eulerian description of phase space dynamics:

(a) Particle simulations [10, 11] are based on the numerical solution of the equations of motion for an ensemble of N_{p} 'superparticles' sampling the phase space dynamics. Each particle represents a trajectory along which the value of f does not change. As N_{p} needs to be much smaller than the actual number of physical particles because of computational limits, this leads to numerical noise (proportional to $N_{\mathrm{p}}^{-1/2}$) which can be reduced but not eliminated by 'δf' [12, 13] and 'split-weight' [14] schemes treating only the fluctuating part $\tilde{f}_{\mathrm{i}} = f_{\mathrm{i}} - f_{\mathrm{i}0}$ or the non-adiabatic part $\tilde{h}_{\mathrm{e}} = f_{\mathrm{e}} - f_{\mathrm{e}0}(1 + e\bar{\phi}/T_{\mathrm{e}})$ of the distribution functions f_{i} and f_{e}. On the other hand, this method is very intuitive and fairly efficient in more than one spatial dimension, provided the small wavelength dynamics are not important. (This is because the required N_{p} is related to the smallest relevant wavelength in the system.) However, to include electromagnetic effects has proven to be difficult [15, 16]. In order to capture the dynamics of kinetic shear Alfvén waves (KSAWs) in the long-wavelength limit, two terms in Ampére's law have to cancel exactly. The inherent particle noise inhibits this cancellation unless the collisionless skin depth c/ω_{pe} ($\rho_{\mathrm{e}} \lesssim c/\omega_{\mathrm{pe}} \lesssim \rho_{\mathrm{i}}$ for typical tokamak parameters with $\mu_{\mathrm{e}} = m_{\mathrm{e}}/m_{\mathrm{i}} \lesssim \beta_{\mathrm{e}} = 4\pi p_{\mathrm{e}}/B^2 \lesssim 1$) is resolved which is numerically prohibitive. Recently, a perturbative approach in μ_{e} was put forward to circumvent this problem [17] but its implementation and testing in three-dimensional toroidal codes has not yet been concluded.

(b) A complementary approach is to adopt a Eulerian point of view and represent f on a grid in five-dimensional phase space [18]. The gyrokinetic dynamics as described by (4)–(7) then advects f past fixed points in phase space. There are two main reasons for considering this

approach instead of particle methods. First, these so-called Vlasov methods do not produce numerical noise, an advantage that is particularly important with respect to fast particles which are generally characterized by low phase space densities but can still have a significant effect on higher-order velocity space moments. Second, it is made sure that all relevant regions of phase space are well represented. For example, if one needs to resolve certain regions in velocity space (say, around Landau resonances or the trapped–passing particle boundary), the grid can be adjusted accordingly. The drawback of Vlasov simulations is that they tend to be computationally expensive due to the use of a grid in velocity space. However, for three-dimensional computations of plasma turbulence both techniques seem to be similarly efficient (see, e.g., the discussion in [19]). Efficiency can also be improved by the use of implicit methods [20] which remove the constraint of explicit codes to resolve the fastest dynamics in the system even if it does not affect the accuracy. The price is a code which is more complex and harder to parallelize (though this has been accomplished [21]). Another way to get an unconditionally stable numerical scheme is by combining the Eulerian and the Lagrangian approaches into a 'semi-Lagrangian' method which traces back the trajectories at every time step, always starting from a regular particle distribution in phase space (see, e.g., [22]).

To keep the numerical effort at a minimum, both Vlasov and particle codes often use a flux-tube geometry employing magnetic-field-aligned coordinates [23, 24]. (However, global ('full radius') simulations are needed to describe radial profile scale effects in a non-perturbative way. For an efficient implementation see, e.g., [25].) But despite these and all of the above conceptual and algorithmic improvements, fairly long simulations on TFlop parallel computers are necessary to obtain well resolved runs in sufficiently large space–time domains. Plasma turbulence therefore ranks among the 'grand challenge' problems of computational physics, and the attempt to include electromagnetic effects makes matters even worse. Through finite-β, KSAWs are introduced which propagate along magnetic field lines with the Alfvén velocity. For typical tokamak values of $\beta_e \sim 1\%$ we have $v_A = c_s/\beta_e^{1/2} \sim 10c_s$. This indicates that the time step has to lowered considerably to resolve the fast Alfvén waves. In explicit codes it is even necessary to resolve the very fast parallel electron dynamics at $v_{te} = c_s/\mu_e^{1/2} \sim 60c_s$ which carries the main part of the parallel current fluctuations causing the magnetic field fluctuations. Due to these constraints and the numerical difficulties mentioned above, only a few nonlinear electromagnetic gyrokinetic codes exist so far (two flux-tube Vlasov codes [19, 20, 26], GS2 (semi-implicit) and GENE (fully explicit), and one flux-tube particle code [27, 28] using a massless electron model [29]) with several other electromagnetic flux-tube and global codes under construction.

3. Electromagnetic effects on microinstabilities

3.1. A simple picture of curvature-driven instabilities

Since many microinstabilities are driven by 'bad' curvature, we will first discuss the corresponding instability mechanism along with finite-β modifications. The dynamics of curvature-driven interchange-like instabilities can generally be described as perpendicular destabilization competing against parallel delocalization. Since a rigorous treatment of curvature-driven instabilities is fairly involved, we will make use of simple analogies. To understand the perpendicular dynamics, we allude to the following situation: an ideal fluid is stratified in terms of its mass density ρ such that ρ decreases with height. This system exhibits undamped waves with frequency $\omega = (g/L_\rho)^{1/2}$ where g is the gravitational constant and $L_\rho = |\mathrm{d}\ln\rho/\mathrm{d}x|^{-1}$ is the mass density scale length. If ρ *increases* with height, we obtain an 'interchange' instability with growth rate $\gamma = (g/L_\rho)^{1/2}$. This observation can be easily

transferred to fusion physics. Plasma particles confined in a toroidal magnetic field are subject to a centrifugal force which can be written in terms of an effective gravitational constant as $g_{\mathrm{eff}} \sim v_{\mathrm{t}}^2/R$ where R is the major radius of the toroidal device. In the outboard midplane the effective gravity points in the direction of decreasing plasma pressure, yielding an instability with the growth rate

$$\gamma \sim (g_{\mathrm{eff}}/L_T)^{1/2} \sim v_{\mathrm{t}}/(RL_T)^{1/2}. \tag{8}$$

Of course, the particles move along the field lines and thus average over different values of the growth rate (which vanishes in the inboard midplane). Therefore a curvature-driven instability depends on mode localization on the outboard side which must be provided by the parallel dynamics. This situation is similar to how one can prevent honey from dripping from a honey dipper [30] by turning it sufficiently fast: there is an instability if and only if the parallel transit frequency is smaller than the interchange growth rate given by (8),

$$\gamma \gtrsim v_{\mathrm{t}}/(qR) \rightarrow R/L_T \gtrsim 1 \tag{9}$$

a condition confirmed by more quantitative analyses. If instead, there is a coupling of perpendicular interchange dynamics to parallel Alfvén wave dynamics, we get

$$\gamma \gtrsim v_{\mathrm{A}}/(qR) \rightarrow \beta \gtrsim \beta_{\mathrm{c}} \tag{10}$$

where $\beta_{\mathrm{c}} \sim L_p/(q^2R)$ is the limit for the onset of the ideal MHD ballooning mode or its gyrokinetic analogue, the kinetic ballooning mode (KBM). At sufficiently large β, the Alfvén wave dynamics is able to control the parallel dynamics instead of the slower ion dynamics, leading to a new electromagnetic instability.

3.2. Linear gyrokinetics of curvature-driven instabilities

To investigate the finite-β effects on curvature-driven instabilities quantitatively, we performed a number of linear runs with GS2 using a local MHD equilibrium [31] with circular flux surfaces and no Shafranov shift. The parameters were $T_{\mathrm{e}}/T_{\mathrm{i}} = 1$, $R/L_n = 2.2$, $q = 1.4$, $\hat{s} = 0.78$, $r/R = 0.18$; no collisions or impurities. Both passing and trapped electrons and ions were included. For $R/L_T = R/L_{T_{\mathrm{e}}} = R/L_{T_{\mathrm{i}}} = 6.9$ the toroidal ion-temperature-gradient (ITG) mode has the largest growth rate at ion scales, $k_\theta \rho_{\mathrm{i}} \lesssim 1$, reaching its maximum value at $k_\theta \rho_{\mathrm{i}} \sim 0.4$ (figure 1). In accord with various other authors, we find that the maximum ITG growth rate drops with increasing β. In our case it is reduced to about 50% of its electrostatic value at $\beta = 2.7\%$. As β is increased further, a KBM is destabilized as can be seen both in the pronounced increase in the maximum growth rate (at $k_\theta \rho_{\mathrm{i}} \sim 0.2$) and in the abrupt change of the corresponding real frequency (in $\hat{s}$–α geometry we would expect to find $\beta_{\mathrm{c}} \approx 2.7\%$ for these parameters). As is explained in the literature (see, e.g., [32] and references therein), finite-β stabilization of ITG modes and the onset of the KBM are closely related, and the KBM can already be destabilized below β_{c}. Trapped electron modes (TEMs) show the same qualitative finite-β behaviour as toroidal ITG modes. This is different from toroidal electron-temperature-gradient (ETG) modes at $k_\theta \rho_{\mathrm{i}} \gg 1$ (figure 1). Here we find that the effect of finite-β is very weak, even across β_{c}, since the parallel localization of the ETG mode is always determined by the fast electron dynamics, not by the slower KSAW dynamics.

3.3. Linear drift-kinetics of collisionless electron drift waves

Although electron drift waves in toroidal geometry are linearly unstable, the resulting turbulence is much like the nonlinear instability found in sheared slab geometry [33]. One further difference between the curvature-driven modes studied in section 3.2 and drift waves

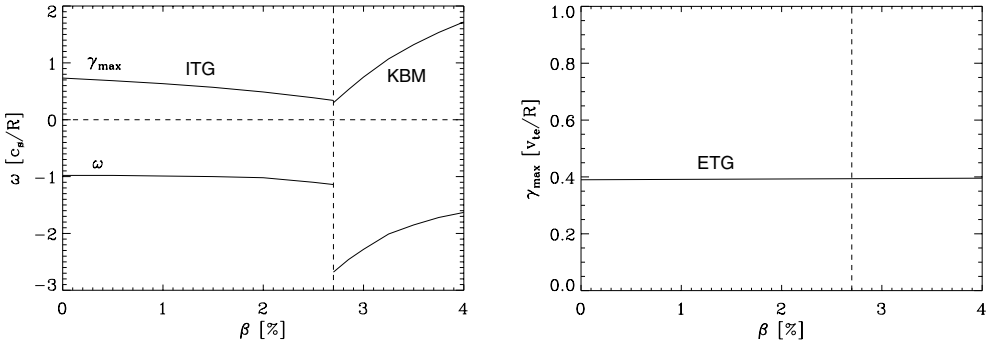

Figure 1. Maximum linear growth rate (and corresponding frequency) for toroidal ITG modes (left) and toroidal ETG modes (right) as a function of β. The dashed line indicates the ideal ballooning limit.

is that the former are reactive whereas the latter are dissipative, i.e. drift waves depend on dissipation (collisions or Landau resonances) in the parallel electron dynamics to drive them to be unstable by producing a non-adiabatic electron response. Therefore the *slowest* dynamics (for a given length scale)—electrons or Alfvén waves—controls non-adiabaticity and hence the drift wave turbulence [3]. From $v_A \lesssim v_{te}$ for $\beta_e \gtrsim \mu_e$ we thus expect that even for $\beta_e \sim \mu_e$ (as is typically found in the edge region of tokamak plasmas) electromagnetic effects can be important. The example shown in figure 3 of [19] is based on an unsheared slab calculation assuming drift-kinetic electrons and cold ions. The parameters were $k_\theta \rho_s = 0.5$ (where ρ_s is the thermal ion gyroradius evaluated at electron temperature), $k_\parallel qR = 1$, $\mu_e (qR/L_n)^2 = 10$, and $R/L_{T_e} = 0$. Indeed, it is found that the growth rate is reduced to about a third of its electrostatic value at $\beta_e = \mu_e$. In the following section we will present nonlinear electromagnetic simulations including effects beyond those captured by linear or naive quasilinear studies.

4. Electromagnetic effects on turbulence and transport

4.1. General considerations

In the 1990s, turbulence in magnetized plasmas came to be seen in terms of a dynamic equilibrium between: (a) isotropic vortices/flows and (b) 'zonal flows' (purely poloidal flows) [34–38] which are self generated by the turbulence and may in turn control it; and (c) 'streamers' (predominantly radial flows) [21, 26] which can lead to very effective radial transport. (Their generation mechanism is still under investigation but it seems to involve both linear and nonlinear physics.) Moreover, extended space–time structures ('avalanches') [39, 40] have been observed which may cause ballistic transport. However, their role under experimentally relevant conditions needs to be further clarified. This dynamic equilibrium has been shown to be fairly sensitive with respect to changes that leave the underlying linear physics invariant. Two prominent examples shall be mentioned here. First, it was discovered that even very low values of ion–ion collisionality (too low to change the linear physics) may affect electrostatic, adiabatic ITG turbulence near the linear threshold [41]. An explanation of this result was given in terms of the collisional damping of zonal flows which tends to enhance the turbulent transport. Second, electrostatic, adiabatic ETG turbulence was found to deviate substantially from its ITG counterpart despite their linear isomorphism [21, 26]. In particular, the ETG

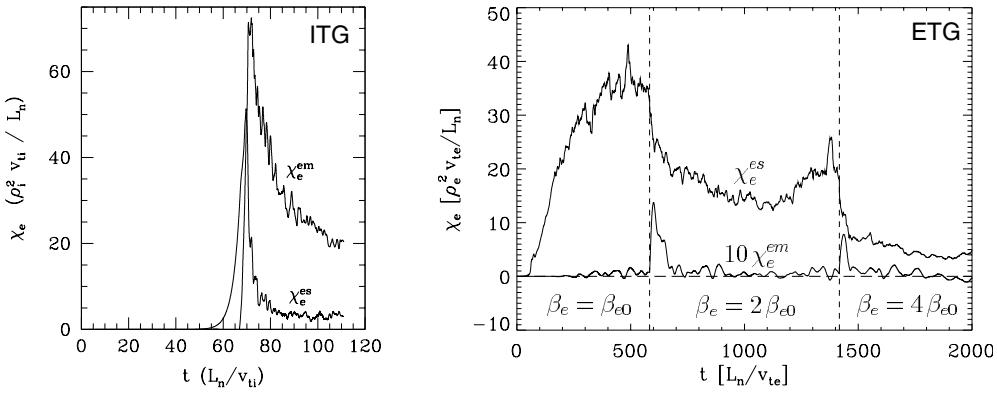

Figure 2. Electrostatic and electromagnetic electron heat transport for gyrokinetic simulations of core ITG/KBM turbulence near the ideal ballooning limit (left) and edge ETG turbulence (right).

system allows for a dominant role of streamers due to the relative weakness of zonal flows at sub-ρ_i scales. In the following subsections we will address the question if there are similar nonlinear effects due to finite-β.

4.2. Toroidal ITG turbulence

Nonlinear GLF simulations of toroidal ITG turbulence [29] have shown that for tokamak core parameters, there can be significant deviations from mixing length theory. The model ignores trapped electrons and treats passing electron dynamics in a small mass ratio expansion. To zeroth order, the electrons are 'frozen in' the magnetic field, and the first-order corrections allow for dissipative effects from electron Landau resonances and electron–ion collisions. It is found that with increasing β the turbulent ion heat transport first exhibits a decrease (as expected from the above linear results), but then a strong increase still below the ideal ballooning limit. Although it has been established that linear expectations are only violated in the presence of electron dissipation, the detailed nonlinear mechanism underlying this kind of behaviour is presently unknown.

Preliminary results from fully gyrokinetic studies seem to support the findings of the GLF simulations. In figure 2, a GS2 simulation of electromagnetic core ITG turbulence is shown. The parameters are the same as in [29] with $\beta = 1.0\%$ where $\beta_c = 1.1\%$. The observed χ_i matches the corresponding GLF result well. In addition, we find that the electron heat transport is dominated by the electromagnetic contribution (see section 4.5 for definitions). This behaviour is likely to be caused either by the linear KBM instability (which is present here despite $\beta < \beta_c$) or the electromagnetic component of the secondary instability (which is found to be significant compared with the electrostatic component). Details will be reported in a future publication.

4.3. Toroidal ETG turbulence

An interesting development in the area of sub-ρ_i-scale turbulence was triggered in 1978 by Ohkawa [42]. General considerations of electron dynamics along perturbed magnetic field lines led him to describe the anomalous electron heat transport by the formula

$$\chi_e \sim \left(\frac{c}{\omega_{pe}}\right)^2 \frac{v_{te}}{qR} \sim \frac{\chi_e^{ml}}{\beta_e}. \tag{11}$$

Interestingly, Ohkawa's prediction for χ_e matched the experimentally observed transport levels much better than the simple mixing length estimate for ETG turbulence, χ_e^{ml}. Subsequently, many authors (see references in [26]) speculated about the possible underlying physics, generally arguing that the turbulent electron heat flux is dominantly caused by magnetic flutter transport at c/ω_{pe} scales.

Nonlinear electromagnetic gyrokinetic simulations of toroidal ETG modes find a different scenario, however. For example, the GENE simulation for tokamak edge parameters ($R/L_n = 27.5$, $\eta_e = 6$, $T_e/T_i = 1$, $q = 3$, $\hat{s} = 1$, $\beta_{e0} = 0.27\%$) shown in figure 2 clearly demonstrates that the transport at sub-ρ_i scales is dominated by $E \times B$ advection. Despite this and the fact that the linear ETG physics does not change significantly with β (as was shown in section 3.2 and confirmed for the present case), an Ohkawa-type transport scaling, $\chi_e \propto 1/\beta_e$, is found. (Note that the value of β_e has been changed twice in the course of the simulation.) The detailed nonlinear mechanism responsible for this behaviour is currently under investigation. (Preliminary results show that the two most obvious candidates are electromagnetic effects on zonal flows and zonal field dynamics.) The β scaling of ETG turbulence might not be universal, however, since a different trend is found for tokamak core parameters [26]. Note that these simulations are computationally very demanding. For example, the run shown in figure 2 took about 150 h on 256 processors on a TFlop computer, the grid in $(x, y, z, v_\parallel, \mu)$ space was $256 \times 256 \times 16 \times 50 \times 10$, corresponding to more than 500 000 000 points in phase space.

4.4. Collisionless drift wave turbulence

In contrast to core turbulence which is characterized by $\omega_{*e} \ll k_\parallel v_A \ll k_\parallel v_{te}$, in the edge these quantities are all of the same order, $\omega_{*e} \sim k_\parallel v_A \sim k_\parallel v_{te}$. Moreover, the magnetic field line excursions away from their equilibrium positions are much more pronounced. Together with the fact that drift waves are subject to a nonlinear instability, this suggests that edge turbulence is extremely complex and rich in nonlinear phenomena. However, some basic insight can be gained by analysing the electromagnetic Ohm's law (first moment of the electron gyrokinetic equation) in slab geometry,

$$m_e n_e \frac{\mathrm{d}\tilde{v}_{e\parallel}}{\mathrm{d}t} = -\tilde{\boldsymbol{b}} \cdot \nabla(\tilde{p}_{e\parallel} - e n_e \tilde{\phi}) - \tilde{\nabla}_\parallel p_{e0} + \frac{e n_e}{c} \frac{\partial \tilde{A}_\parallel}{\partial t} \tag{12}$$

where $\tilde{\boldsymbol{b}} \cdot \nabla = \nabla_\parallel + \tilde{\nabla}_\parallel$. Here, $\tilde{}$ and the subscript '0' denote perturbed and equilibrium quantities, respectively, with the exception of $\tilde{\boldsymbol{b}}$ which is the unit vector along perturbed magnetic field lines. Using Ampére's law, it can be easily shown that for $k_\perp(c/\omega_{pe}) \lesssim 1$, the term of the left-hand side is small compared with the induction term $\partial_t \tilde{A}_\parallel$. However, for $\omega \sim \omega_{*e}$, the latter tends to be cancelled by the linear flutter term $\tilde{\nabla}_\parallel p_{e0}$, so that the net electromagnetic effect on electron non-adiabaticity and drift wave instability may be dominated by the nonlinear flutter terms contained in the first term on the right-hand side of (12). Although finite T_e gradients and toroidal effects break this cancellation, the observed β dependence of drift wave turbulence in both gyrokinetic and GLF simulations is generally rather weak [43, 44]. Thus the relatively pronounced linear stabilization observed in section 3.3 does not carry over into the nonlinear regime, and careful nonlinear studies of electromagnetic tokamak edge turbulence are required to investigate the possible role of β as a trigger for the L–H transition.

4.5. Turbulent transport

Despite all the above electromagnetic effects on various kinds of plasma turbulence, the induced transport is predominantly electrostatic in nature [3, 45] except close to the ideal ballooning

limit (see figure 2). To understand this somewhat surprising finding, we briefly analyse the magnetic flutter contribution to the turbulent radial heat flux,

$$Q_j^{\mathrm{em}} = \langle \tilde{q}_{j\parallel} \tilde{B}_r \rangle / B_0 \tag{13}$$

where $j = \mathrm{e}, \mathrm{i}$ is the species index and angular brackets denote spatial averaging. It adds to the electrostatic contribution $Q_j^{\mathrm{es}} = (3/2)\langle \tilde{p}_j \tilde{v}_{Er} \rangle$ and is due to parallel heat conduction along fluctuating magnetic field lines. (In a system that is periodic in both perpendicular directions (which is true for most flux-tube simulations including the ones presented in this paper) there is no flutter contribution to the radial particle transport.) For $\omega \ll k_\parallel v_{\mathrm{t}j}$, the parallel heat flux can in turn be written as

$$\tilde{q}_{j\parallel} = -n\chi_{j\parallel} \tilde{\boldsymbol{b}} \cdot \nabla T_{j\parallel} = -n\chi_{j\parallel} \left[\nabla_\parallel \tilde{T}_{j\parallel} + \tilde{\nabla}_\parallel \tilde{T}_{j\parallel} + \left(\frac{\tilde{B}_r}{B_0} \right) \left(\frac{\mathrm{d}T_{j0}}{\mathrm{d}r} \right) \right] \tag{14}$$

with $\chi_{j\parallel} \approx L_0 v_{\mathrm{t}j}$ where L_0 is a characteristic parallel scale length. From $v_{\mathrm{ti}} \ll v_{\mathrm{te}}$ it is clear that the ions do not contribute much compared with the electrons, but nonlinear simulations typically find $Q_{\mathrm{e}}^{\mathrm{em}} \ll Q_{\mathrm{e}}^{\mathrm{es}}$. This is due to the fact that the first term on the right-hand side of (14) usually dominates so that $\tilde{q}_{\mathrm{e}\parallel}$ and $\tilde{B}_r$ tend to be uncorrelated. As the ideal ballooning limit is approached, however, the other two terms in (14) dominate so that there is now a strong correlation between $\tilde{q}_{\mathrm{e}\parallel}$ and $\tilde{B}_r$. Henceforth one expects a significant contribution from magnetic flutter transport in this case as is indeed observed in simulations of electromagnetic ITG turbulence (see figure 2). Since test particle calculations (see, e.g., [46] and references therein) are not self-consistent and often only keep the third term on the right-hand side of (14) (leading to $\chi_{\mathrm{e}}^{\mathrm{em}} \approx \chi_{\mathrm{e}\parallel} \langle (\tilde{B}_r / B_0)^2 \rangle$), they tend to overestimate the magnetic flutter transport.

5. Synopsis and outlook

Due to the importance of kinetic and finite-β effects, plasma turbulence on closed field lines should be described by electromagnetic gyrokinetic (or gyro-Landau-fluid) models to obtain more realistic results. Linearly, electromagnetic effects on primarily electrostatic microinstabilities are generally weakly to moderately stabilizing. However, fully developed turbulence driven by ITG modes, ETG modes, and electron drift waves can be dominated by nonlinear electromagnetic effects and yield surprising results not in line with linear or naive quasilinear expectations. Examples for this are the strong increase of transport at ρ_{i} scales well below the ideal ballooning limit, an Ohkawa-type scaling of electron heat transport at sub-ρ_{i} scales, and the relative insensitivity of edge turbulence with respect to β. In contrast to test particle calculations, the induced transport is generally electrostatic in nature well below the ideal ballooning limit.

Despite the challenging nature of nonlinear electromagnetic gyrokinetic simulations both in terms of algorithm development and computational requirements, there has been significant progress over the last few years. Preliminary results indicate that there is much interesting and relevant finite-β physics to unravel. With many new electromagnetic gyrokinetic codes under construction, it can be anticipated that we will thus get closer to an accurate description of turbulent transport in fusion devices.

Acknowledgments

We would like to thank G W Hammett and B Scott for helpful suggestions and the careful reading of the manuscript. The nonlinear simulations were performed at the Leibniz Computing Center and the US National Energy Research Supercomputing Center.

References

[1] Tennekes H and Lumley J L 1972 *A First Course in Turbulence* (Cambridge: MIT Press)
[2] Hasegawa A 1985 *Adv. Phys.* **34** 1
[3] Scott B D 1997 *Plasma Phys. Control. Fusion* **39** 1635
[4] Jenko F and Scott B D 1998 *Phys. Rev. Lett.* **80** 4883
[5] Hammett G W and Perkins F W 1990 *Phys. Rev. Lett.* **64** 3019
[6] Antonsen T and Lane B 1980 *Phys. Fluids* **23** 1205
[7] Frieman E A and Chen L 1982 *Phys. Fluids* **25** 502
[8] Hahm T S, Lee W W and Brizard A 1988 *Phys. Fluids* **31** 1940
[9] Brizard A 1989 *J. Plasma Phys.* **41** 541
[10] Dawson J M 1983 *Rev. Mod. Phys.* **55** 403
[11] Birdsall C K and Langdon A B 1985 *Plasma Physics via Computer Simulation* (New York: McGraw-Hill)
[12] Kotschenreuther M 1988 *Bull. Am. Phys. Soc.* **34** 2107
Denton R E and Kotschenreuther M 1995 *J. Comput. Phys.* **119** 283
[13] Dimits A M and Lee W W 1993 *J. Comput. Phys.* **107** 309
[14] Manuilskiy I and Lee W W 2000 *Phys. Plasmas* **7** 1381
[15] Reynders J V W 1992 *PhD Thesis* Princeton University
[16] Cummings J C 1995 *PhD Thesis* Princeton University
[17] Lin Z and Chen L 2001 *Phys. Plasmas* **8** 1447
[18] Armstrong T P, Harding R C, Knorr G and Montgomery D 1970 *Methods of Computational Physics* vol 9, ed B Aider, S Fembach and M Rotenberg (New York: Academic) p 29
[19] Jenko F 2000 *Comput. Phys. Commun.* **125** 196
[20] Kotschenreuther M, Rewoldt G and Tang W M 1995 *Comput. Phys. Commun.* **88** 128
[21] Dorland W, Jenko F, Kotschenreuther M and Rogers B N 2000 *Phys. Rev. Lett.* **85** 5579
[22] Sonnendrücker E, Roche J, Bertrand P and Ghizzo A 1999 *J. Comput. Phys.* **149** 201
[23] Cowley S C, Kulsrud R M and Sudan R 1991 *Phys. Fluids* B **3** 2767
[24] Beer M A, Cowley S C and Hammett G W 1995 *Phys. Plasmas* **2** 2687
[25] Fivaz M, Brunner S, de Ridder G, Sauter O, Tran T M, Vaclavik J, Villard L and Appert K 1998 *Comput. Phys. Commun.* **111** 27
[26] Jenko F, Dorland W, Kotschenreuther M and Rogers B N 2000 *Phys. Plasmas* **7** 1904
[27] Parker S E, Chen Y and Kim C C 2000 *Comput. Phys. Commun.* **127** 59
[28] Chen Y and Parker S E 2001 *Phys. Plasmas* **8** 441
[29] Snyder P B and Hammett G W 2001 *Phys. Plasmas* **8** 744
[30] Hammett G W 1999 *Bull. Am. Phys. Soc.* **44** 1645
[31] Miller R L, Chu M S, Greene J M, Lin-Liu Y R and Waltz R E 1998 *Phys. Plasmas* **5** 973
[32] Kim J Y, Horton W and Dong J Q 1993 *Phys. Fluids* B **5** 4030
[33] Scott B D 1990 *Phys. Rev. Lett.* **65** 3289
[34] Hasegawa A and Wakatani M 1987 *Phys. Rev. Lett.* **59** 1581
[35] Carreras B A, Lynch V E and Garcia L 1991 *Phys. Fluids* B **3** 1438
[36] Diamond P H and Kim Y B 1991 *Phys. Fluids* B **3** 1626
[37] Hammett G W, Beer M A, Dorland W, Cowley S C and Smith S A 1993 *Plasma Phys. Control. Fusion* **35** 973
[38] Cohen B I, Williams T J, Dimits A M and Byers J A 1993 *Phys. Fluids* B **5** 2967
[39] Garbet X and Waltz R E 1998 *Phys. Plasmas* **5** 2836
[40] Sarazin Y and Ghendrih P 1998 *Phys. Plasmas* **5** 4214
[41] Lin Z, Hahm T S, Lee W W, Tang W M and Diamond P H 1999 *Phys. Rev. Lett.* **83** 3645
[42] Ohkawa T 1978 *Phys. Lett.* **67A** 35
[43] Jenko F and Scott B D 1999 *Phys. Plasmas* **6** 2705
[44] Scott B 1998 *Theory of Fusion Plasmas* ed J Connor, E Sindoni and J Vaclavik (Bologna: Editrice Compositori) p 359
[45] Waltz R E 1985 *Phys. Fluids* **28** 577
[46] Krommes J A, Oberman C and Kleva R G 1983 *J. Plasma Phys.* **30** 11